

# Structure of Vector Mesons in Holographic Model with Linear Confinement

H.R. Grigoryan<sup>1,2</sup> and A.V. Radyushkin<sup>1,3,4</sup>

<sup>1</sup>*Thomas Jefferson National Accelerator Facility, Newport News, VA 23606, USA*

<sup>2</sup>*Physics Department, Louisiana State University, Baton Rouge, LA 70803, USA*

<sup>3</sup>*Physics Department, Old Dominion University, Norfolk, VA 23529, USA*

<sup>4</sup>*Laboratory of Theoretical Physics, JINR, Dubna, Russian Federation*

Wave functions and form factors of vector mesons are investigated in the holographic dual model of QCD with oscillator-like infrared cutoff. We introduce wave functions conjugate to solutions of the 5D equation of motion and develop a formalism based on these wave functions, which are very similar to those of a quantum-mechanical oscillator. For the lowest bound state ( $\rho$ -meson), we show that, in this model, the basic elastic form factor exhibits the perfect vector meson dominance, i.e., it is given by the  $\rho$ -pole contribution alone. The electric radius of the  $\rho$ -meson is calculated,  $\langle r_\rho^2 \rangle_C = 0.655 \text{ fm}^2$ , which is larger than in case of the hard-wall cutoff. The squared radii of higher excited states are found to increase logarithmically rather than linearly with the radial excitation number. We calculate the coupling constant  $f_\rho$  and find that the experimental value is closer to that calculated in the hard-wall model.

PACS numbers: 11.25.Tq, 11.10.Kk, 11.25.Wx,

## I. INTRODUCTION

Holographic duals of quantum chromodynamics (QCD) which are based on the gauge/gravity correspondence [1] have been applied recently to hadronic physics (see, e.g., [2, 3, 4, 5, 6, 7, 8, 9, 10, 11, 12, 13, 14]), and demonstrated their ability to incorporate such essential properties of QCD as confinement and chiral symmetry breaking, and have been successful in many cases in determination of static hadronic properties, i.e., resonance masses, decay constants, chiral coefficients, etc. In Refs. [2, 4], the dynamic properties (form factors) have been studied within the holographic approach of Ref. [2], and the connection between AdS/QCD approach of Refs. [2, 4] and the usual light-cone formalism for hadronic form factors was proposed in [11] and discussed in [15]. The calculation of form factors of scalar and vector hadrons within the approach of Ref. [2] was performed in Refs. [16, 17], and applied to study the universality of the  $\rho$ -meson couplings to other hadrons. In our recent paper [18], we studied form factors and wave functions of vector mesons within the framework of the holographic QCD model described in Refs. [6, 7, 8] (which will be referred to as hard-wall model).

In the hard-wall model, the confinement is modeled by hard-wall cutting off the AdS space along the extra fifth dimension at some finite value  $z = z_0$ . The solutions of the relevant eigenvalue equation are given by the Bessel functions, and masses of bound states are given by the roots  $M_n = \gamma_{0,n}/z_0$  of  $J_0(Mz_0)$ . As a result, the masses of higher excitations behave like  $M_n^2 \sim n^2$ . It was argued [12, 19] that, instead, one should expect  $M_n^2 \sim n$  behavior. This connection can be derived from semiclassical arguments [19, 20]. An explicit AdS/QCD model which gives such a linear behavior was proposed in Ref. [12]. The hard-wall boundary conditions in this model are substituted by an oscillator-type potential providing a soft IR cut-off in the action integral (for this reason, it will

be referred to as “soft-wall model”).

The aim of the present paper is to study form factors and wave functions of vector mesons within the framework of the soft-wall model formulated in Ref. [12], and compare the results with those we obtained in Ref. [18] investigating the hard-wall model. To this end, we extend the approach developed in Ref. [18]. We start with recalling, in Section II, the basics of the soft-wall model and some results obtained in Ref. [12], in particular, the form of the relevant action, the eigenvalue equation for bound states and its solution. In Section III, we derive a useful integral representation for the bulk-to-boundary propagator  $\mathcal{V}(p, z)$  that allows to write  $\mathcal{V}(p, z)$  as an explicit expansion over bound state poles with the  $z$ -dependence of each pole contribution given by “ $\psi$  wave functions” that are eigenfunctions of the 5D equation of motion. Then we show that the same representation can be obtained from the general formalism of Green’s functions. However, as we already emphasized in Ref. [18], the  $\psi_n(z)$  wave functions are not direct analogues of the usual quantum-mechanical wave functions. In particular, a meson coupling constant  $f_n$  is obtained from the derivative of  $\psi_n(z)$  at  $z = 0$  rather than from its value at this point. To this end, we introduce “ $\phi$  wave functions” which look more like wave functions of oscillator bound states in quantum mechanics. Their values at  $z = 0$  give the bound state couplings  $g_5 f_n/M_n$ , they exponentially decrease with  $z^2$ , and thus they have properties necessary for the light-cone interpretation of AdS/QCD results proposed in Ref. [11]. In Section IV, we study the three-point function  $\langle JJJ \rangle$  and obtain expression for transition form factors that involves  $\psi$  wave functions and the nonnormalizable mode factor  $\mathcal{J}(Q, z)$ . The latter is written as a sum over all bound states in the channel of electromagnetic current, which gives an analogue of generalized vector meson dominance (VMD) representation for hadronic form factors. In Section V, it is shown that it is possible to rewrite form factors in terms of  $\phi$  functions. Then we formu-

late predictions for  $\rho$ -meson form factors, and analyze these predictions in the regions of small and large  $Q^2$ . In particular, our formalism allows to calculate  $\rho$ -meson electric radius, and the radii of higher excited states. It is also shown that, for the basic  $\rho$ -meson form factor  $\mathcal{F}(Q^2)$  given by the overlap of the  $\phi$  wave functions, the soft-wall model predicts exact VMD pattern, when just one lowest bound state in the  $Q^2$ -channel contributes. For another  $\rho$ -meson form factor  $F(Q^2)$ , which is given by the overlap of the  $\psi$  wave functions, a two-resonance dominance is established, with only two lowest bound states in the  $Q^2$ -channel contributing. In Section VI, we compare our results obtained in the soft-wall model with those derived in the hard-wall model studies performed in Ref. [18]. At the end, we summarize the paper.

## II. PRELIMINARIES

We consider the gravity background with a smooth cutoff that was proposed in Ref. [12] instead of a hard-wall infrared (IR) cutoff. In this case, the only background fields are dilaton  $\chi(z) = z^2\kappa^2$  and metric  $g_{MN}$ . The metric can be written as

$$g_{MN}dx^M dx^N = \frac{1}{z^2} (\eta_{\mu\nu} dx^\mu dx^\nu - dz^2) , \quad (1)$$

where  $\eta_{\mu\nu} = \text{Diag}(1, -1, -1, -1)$  and  $\mu, \nu = (0, 1, 2, 3)$ ,  $M, N = (0, 1, 2, 3, z)$ . To determine the spectrum of vector mesons, one needs the quadratic part of the action

$$S_{\text{AdS}} = -\frac{1}{4g_5^2} \int d^4x \frac{dz}{z} e^{-\chi} \text{Tr} (F_{MN} F^{MN}) , \quad (2)$$

where  $F_{MN} = \partial_M V_N - \partial_N V_M - i[V_M, V_N]$ ,  $V_M = t^a V_M^a$ , ( $t^a = \sigma^a/2$ , with  $\sigma^a$  being Pauli matrices). In the axial-like gauge  $V_z = 0$ , the vector field  $V_\mu^a(x, z = 0)$  corresponds to the source for the vector current  $J_\mu^a(x)$ . To obtain the equations of motion for the transverse component of the field, it is convenient to work with the Fourier transform  $\tilde{V}_\mu^a(p, z)$  of  $V_\mu^a(x, z)$ , for which one has

$$\left( \partial_z \left[ \frac{1}{z} e^{-z^2} \partial_z \tilde{V}_\mu^a(p, z) \right] + p^2 \frac{1}{z} e^{-z^2} \tilde{V}_\mu^a(p, z) \right) \Big|_{\perp} = 0 . \quad (3)$$

(Here, and in the rest of the paper, we find it convenient to follow the convention of Ref. [12], in which the oscillator scale  $\kappa$  is treated as 1, i.e., we write below  $z^2$  instead of  $\kappa^2 z^2$ ,  $e^{-z^2}$  instead of  $e^{-z^2\kappa^2}$ , etc. Using dimensional analysis, the reader can easily restore the hidden factors of  $\kappa$  in our expressions. In some cases, when  $\kappa$  is not accompanied by  $z$ , we restore  $\kappa$  explicitly.) The eigenvalue equation for wave functions  $\psi_n(z)$  of the normalizable modes can be obtained from Eq. (3) by requiring  $p^2 = M_n^2$ , which gives

$$\partial_z \left[ \frac{1}{z} e^{-z^2} \partial_z \psi_n \right] + M_n^2 \frac{1}{z} e^{-z^2} \psi_n = 0 . \quad (4)$$

As noted in Ref. [12], the substitution

$$\psi_n(z) = e^{z^2/2} \sqrt{z} \Psi_n(z) \quad (5)$$

gives a Schrödinger equation

$$-\Psi_n'' + \left( z^2 + \frac{3}{4z^2} \right) \Psi_n = M_n^2 \Psi_n , \quad (6)$$

which happens to be exactly solvable. The resulting spectrum is  $M_n^2 = 4(n+1)$  (with  $n = 0, 1, \dots$ ), and the solutions  $\psi_n(z)$  of the original equation (4) are given by

$$\psi_n(z) = z^2 \sqrt{\frac{2}{n+1}} L_n^1(z^2) , \quad (7)$$

where  $L_n^1(z^2)$  are Laguerre polynomials. The functions  $\psi_n(z)$  are normalized according to

$$\int_0^\infty \frac{dz}{z} e^{-z^2} \psi_m(z) \psi_n(z) = \delta_{mn} . \quad (8)$$

Correspondingly, the  $\Psi_n(z)$  functions of the Schrödinger equation (6) are normalized by

$$\int_0^\infty dz \Psi_m(z) \Psi_n(z) = \delta_{mn} , \quad (9)$$

i.e., just like wave functions of bound states in quantum mechanics. Note, however, that the functions  $\Psi_n(z)$  behave like  $z^{3/2}$  for small  $z$ , while quantum-mechanical wave functions of bound states with zero angular momentum have finite non-zero values at the origin.

## III. BULK-TO-BOUNDARY PROPAGATOR

It is convenient to represent  $\tilde{V}_\mu^a(p, z)$  as the product of the 4-dimensional boundary field  $\tilde{V}_\mu^a(p)$  and the bulk-to-boundary propagator  $\mathcal{V}(p, z)$  which obeys the basic equation

$$\partial_z \left[ \frac{1}{z} e^{-z^2} \partial_z \mathcal{V} \right] + p^2 \frac{1}{z} e^{-z^2} \mathcal{V} = 0 \quad (10)$$

that follows from Eq. (3) and satisfies the boundary condition

$$\mathcal{V}(p, z = 0) = 1 . \quad (11)$$

Its general solution is given by the confluent hypergeometric functions of the first and second kind

$$\mathcal{V}(p, z) = A {}_1F_1(a, 0, z^2) + B U(a, 0, z^2) , \quad (12)$$

where  $a = -p^2/4\kappa^2$ ,  $A$  and  $B$  are constants. Since the function  ${}_1F_1(a, 0, z^2)$  is singular for  $z = 0$ , we take  $A = 0$ . Then, for  $a > 0$ , the bulk-to-boundary propagator  $\mathcal{V}(p, z)$  can be written as

$$\mathcal{V}(p, z) = a \int_0^1 dx x^{a-1} \exp \left[ -\frac{x}{1-x} z^2 \right] . \quad (13)$$

It is easy to check that this expression satisfies Eqs. (10) and (11). Integrating by parts produces the representation

$$\mathcal{V}(p, z) = z^2 \int_0^1 \frac{dx}{(1-x)^2} x^a \exp\left[-\frac{x}{1-x} z^2\right], \quad (14)$$

from which it follows that if  $p^2 = 0$  (or  $a = 0$ ), then

$$\mathcal{V}(0, z) = 1 \quad (15)$$

for all  $z$ . The integrand of Eq. (14) contains the generating function

$$\frac{1}{(1-x)^2} \exp\left[-\frac{x}{1-x} z^2\right] = \sum_{n=0}^{\infty} L_n^1(z^2) x^n \quad (16)$$

for the Laguerre polynomials  $L_n^1(z^2)$ , which gives the representation

$$\mathcal{V}(p, z) = z^2 \sum_{n=0}^{\infty} \frac{L_n^1(z^2)}{a+n+1} \quad (17)$$

that can be analytically continued into the timelike  $a < 0$  region. One can see that  $\mathcal{V}(p, z)$  has poles there at expected locations  $p^2 = 4(n+1)\kappa^2$ .

The same representation for  $\mathcal{V}(p, z)$  can be obtained from the Green's function

$$G(p; z, z') = \sum_{n=0}^{\infty} \frac{\psi_n(z)\psi_n(z')}{p^2 - M_n^2} \quad (18)$$

corresponding to Eq. (10), namely,

$$\begin{aligned} \mathcal{V}(p, z') &= - \left[ \frac{1}{z'} e^{-z'^2} \partial_{z'} G(p; z, z') \right]_{z=\epsilon \rightarrow 0} \\ &= - \sum_{n=0}^{\infty} \frac{\sqrt{8(n+1)}\psi_n(z')}{p^2 - M_n^2} = -4 \sum_{n=0}^{\infty} \frac{z'^2 L_n^1(z'^2)}{p^2 - M_n^2}, \end{aligned} \quad (19)$$

which coincides with Eq. (17).

The two-point density function can also be obtained from the Green's function:

$$\begin{aligned} \Sigma(p^2) &= \frac{1}{g_5^2} \left[ \frac{1}{z'} e^{-z'^2} \partial_{z'} \left[ \frac{1}{z} e^{-z^2} \partial_z G(p; z, z') \right] \right]_{z, z'=\epsilon \rightarrow 0} \\ &= \sum_{n=0}^{\infty} \frac{f_n^2}{p^2 - M_n^2}, \end{aligned} \quad (20)$$

where the coupling constants  $f_n = \kappa^2 \sqrt{8(n+1)}/g_5$  obtained in [12] are determined by

$$f_n = \frac{1}{g_5 z} e^{-z^2} \partial_z \psi_n(z) \Big|_{z=\epsilon \rightarrow 0}. \quad (21)$$

The propagator  $\mathcal{V}(p, z)$  can be represented now as

$$\mathcal{V}(p, z) = g_5 \sum_{n=0}^{\infty} \frac{f_n \psi_n(z)}{M_n^2 - p^2}, \quad (22)$$

where  $\psi_n(z)$  are the original wave functions (7) corresponding to the solutions of the eigenvalue equation (4).

Given the structure of Eq. (21), it is natural to introduce the conjugate wave functions

$$\begin{aligned} \phi_n(z) &\equiv \frac{1}{M_n z} e^{-z^2} \partial_z \psi_n(z) \\ &= \frac{2}{M_n} e^{-z^2} [L_n^1(z^2) - z^2 L_{n-1}^2(z^2)], \end{aligned} \quad (23)$$

whose nonzero values at the origin  $f_n g_5 / M_n$  are proportional to the coupling constant  $f_n$  (in this particular case,  $f_n g_5 / M_n = \sqrt{2}\kappa$ ). The inverse relation between the  $\psi$  and  $\phi$  wave functions

$$\psi_n(z) = -\frac{1}{M_n} z e^{z^2} \partial_z \phi_n(z) \quad (24)$$

can be obtained from Eq. (4). The  $\phi$ -functions are normalized by

$$\int_0^{\infty} dz z e^{z^2} \phi_m(z) \phi_n(z) = \delta_{mn}. \quad (25)$$

In particular, for the lowest states, we have

$$\phi_0(z) = \sqrt{2} e^{-z^2}, \quad \phi_1(z) = \sqrt{2} e^{-z^2} (1 - z^2). \quad (26)$$

Just like zero angular momentum oscillator wave functions in quantum mechanics, these functions have finite values at  $z = 0$ . They also have a Gaussian fall-off  $e^{-z^2}$  for large  $z$ . To make a more close analogy with the oscillator wave functions, it makes sense to absorb the weight  $e^{z^2}$  in Eq. (25) into the wave functions, i.e., to introduce “ $\Phi$ ” wave functions

$$\Phi_n(z) \equiv e^{z^2/2} \phi_n(z) = \frac{1}{M_n z} e^{-z^2/2} \partial_z \psi_n(z), \quad (27)$$

which are nonzero at  $z = 0$ , decrease like  $e^{-z^2/2}$  for large  $z$ , and are normalized according to

$$\int_0^{\infty} dz z \Phi_m(z) \Phi_n(z) = \delta_{mn}. \quad (28)$$

The presence of the  $z$  weight in this condition (which cannot be absorbed into wave functions without spoiling their behavior at  $z = 0$ ) suggests that pursuing the analogy with quantum mechanics one should treat  $z$  as the radial variable of a 2-dimensional quantum mechanical system.

#### IV. 3-POINT FUNCTION

The variation of the trilinear (in  $V$ ) term of the action

$$S_{\text{AdS}}^{(3)} = -\frac{\epsilon_{abc}}{2g_5^2} \int d^4x \int_{\epsilon}^{\infty} \frac{dz}{z} e^{-z^2} (\partial_{\mu} V_{\nu}^a) V^{\mu, b} V^{\nu, c} \quad (29)$$

calculated on the solutions of the basic equation (10) gives the following result for the 3-point correlator:

$$\langle J_a^\alpha(p_1) J_b^\beta(-p_2) J_c^\mu(q) \rangle = \epsilon_{abc} (2\pi)^4 \frac{2i}{g_5^2} \delta^{(4)}(p_1 - p_2 + q) \\ \times T^{\alpha\beta\mu}(p_1, p_2, q) W(p_1, p_2, q), \quad (30)$$

with the dynamical part given by

$$W(p_1, p_2, q) \equiv \int_\epsilon^\infty \frac{dz}{z} e^{-z^2} \mathcal{V}(p_1, z) \mathcal{V}(p_2, z) \mathcal{V}(q, z), \quad (31)$$

and the kinematical factor having the structure of a non-abelian three-field vertex:

$$T^{\alpha\beta\mu}(p_1, p_2, q) = \eta^{\alpha\mu}(q - p_1)^\beta - \eta^{\beta\mu}(p_2 + q)^\alpha \\ + \eta^{\alpha\beta}(p_1 + p_2)^\mu. \quad (32)$$

Incorporating the representation Eq. (22) for the bulk-to-boundary propagators gives the expression

$$T(p_1^2, p_2^2, Q^2) = \sum_{n,k=1}^{\infty} \frac{f_n f_k F_{nk}(Q^2)}{(p_1^2 - M_n^2)(p_2^2 - M_k^2)} \quad (33)$$

for  $T(p_1^2, p_2^2, Q^2) \equiv W(p_1, p_2, q)/g_5^2$  as a sum over the poles of the bound states in the initial and final states. In the  $z$ -integral of Eq. (31), the contribution of each bound state is accompanied by its wave function  $\psi_n(z)$ , while the  $q$ -channel is represented by  $\mathcal{J}(Q, z) = \mathcal{V}(iQ, z)$ . This gives the  $Q^2$ -dependent coefficients

$$F_{nk}(Q^2) = \int_0^\infty \frac{dz}{z} e^{-z^2} \mathcal{J}(Q, z) \psi_n(z) \psi_k(z), \quad (34)$$

which have the meaning of transition form factors. Note that since  $\mathcal{J}(0, z) = 1$ , the orthonormality relation (8) assures that  $F_{nn}(Q^2 = 0) = 1$  for diagonal transitions and  $F_{nk}(Q^2 = 0) = 0$  if  $n \neq k$ .

The factor  $\mathcal{J}(Q, z)$  can be written as a sum of monopole contributions from the infinite tower of vector mesons:

$$\mathcal{J}(Q, z) = g_5 \sum_{m=1}^{\infty} \frac{f_m \psi_m(z)}{Q^2 + M_m^2}. \quad (35)$$

This decomposition, discussed in Refs. [16, 18], directly follows from Eq. (22). As a result, the form factors  $F_{nk}(Q^2)$  can be written in the form of a generalized VMD representation:

$$F_{nk}(Q^2) = \sum_{m=1}^{\infty} \frac{F_{m,nk}}{1 + Q^2/M_m^2}, \quad (36)$$

where the coefficients  $F_{m,nk}$  are given by the overlap integrals

$$F_{m,nk} = \frac{g_5 f_m}{M_m^2} \int_0^\infty \frac{dz}{z} e^{-z^2} \psi_m(z) \psi_n(z) \psi_k(z). \quad (37)$$

## V. FORM FACTORS

In terms of the  $\Psi$  wave functions of the Schrödinger equation (6), the form factors are given by

$$F_{nk}(Q^2) = \int_0^\infty dz \mathcal{J}(Q, z) \Psi_n(z) \Psi_k(z), \quad (38)$$

which looks like an expression for form factors in quantum mechanics. However, as we discussed above, the  $\Psi$  wave functions are not direct analogues of quantum mechanical wave functions. For such an analogy, the  $\Phi$  wave functions (27) are much more suitable objects. So, let us introduce form factors involving  $\Phi$  wave functions

$$\mathcal{F}_{nk}(Q^2) \equiv \int_0^\infty dz z \mathcal{J}(Q, z) \Phi_n(z) \Phi_k(z). \quad (39)$$

Again, since  $\mathcal{J}(Q = 0, z) = 1$  for all  $z$ , the normalization condition (28) for the  $\Phi_n(z)$  wave functions guarantees that the diagonal form factors  $\mathcal{F}_{nn}(Q^2)$  are normalized to 1 for  $Q^2 = 0$ , while the non-diagonal ones vanish when  $Q^2 = 0$ . To establish connection with  $F_{nk}(Q^2)$  form factors, we use Eq. (27) to substitute  $\Phi$  functions by derivatives of  $\psi$  wave functions, which gives

$$M_n M_k \mathcal{F}_{nk}(Q^2) = \int_0^\infty \frac{dz}{z} e^{-z^2} \mathcal{J}(Q, z) \psi'_n(z) \psi'_k(z). \quad (40)$$

Integrating  $\psi'_k$  by parts, taking into account that  $\psi_k(0) = 0$  and incorporating the eigenvalue equation (4) for  $\psi_n$  gives

$$M_n M_k \mathcal{F}_{nk}(Q^2) = M_n^2 F_{nk}(Q^2) \\ - \int_0^\infty \frac{dz}{z} e^{-z^2} \psi'_n(z) \psi_k(z) \partial_z \mathcal{J}(Q, z). \quad (41)$$

Similarly, integrating  $\psi'_n$  by parts we obtain

$$M_n M_k \mathcal{F}_{nk}(Q^2) = M_k^2 F_{nk}(Q^2) \\ - \int_0^\infty \frac{dz}{z} e^{-z^2} \psi_n(z) \psi'_k(z) \partial_z \mathcal{J}(Q, z). \quad (42)$$

Adding these two expressions, integrating  $(\psi_n \psi_k)'$  by parts and using the basic equation (10) for  $\mathcal{J}(Q, z)$  gives

$$F_{nk}(Q^2) = \frac{2M_n M_k}{Q^2 + M_n^2 + M_k^2} \mathcal{F}_{nk}(Q^2). \quad (43)$$

For the case of diagonal  $n \rightarrow n$  transitions this gives

$$F_{nn}(Q^2) = \frac{\mathcal{F}_{nn}(Q^2)}{1 + Q^2/2M_n^2}, \quad (44)$$

expression similar to that derived in Ref. [18].

Thus, we can obtain  $F_{nk}(Q^2)$  form factors from the basic form factors  $\mathcal{F}_{nk}(Q^2)$ . Note, that these form factors also have a generalized VMD representation

$$\mathcal{F}_{nk}(Q^2) = \sum_{m=1}^{\infty} \frac{\mathcal{F}_{m,nk}}{1 + Q^2/M_m^2}, \quad (45)$$

with the coefficients  $\mathcal{F}_{m,nk}$  given by the overlap integrals

$$\mathcal{F}_{m,nk} = \frac{g_5 f_m}{M_m^2} \int_0^\infty dz z \psi_m(z) \Phi_n(z) \Phi_k(z). \quad (46)$$

For the lowest diagonal transition (i.e., for  $n = k = 0$ ) we have

$$\mathcal{F}_{00}(Q^2) = 2 \int_0^\infty dz z e^{-z^2} \mathcal{J}(Q, z). \quad (47)$$

Incorporating the representation (14) for  $\mathcal{J}(Q, z)$  and using  $a = Q^2/4\kappa^2$ , we obtain

$$\mathcal{F}_{00}(Q^2) = \frac{1}{1+a} = \frac{1}{1+Q^2/M_0^2}. \quad (48)$$

Here, we took into account that the mass of the lowest bound state (i.e.,  $\rho$ -meson) is  $M_0 = M_\rho = 2\kappa$ .

Notice, that we obtained exact vector meson dominance for  $\mathcal{F}_{00}(Q^2)$ : this form factor is completely determined by the lowest bound state in the  $q$ -channel. The higher states do not contribute because the overlap integral  $\mathcal{F}_{m,00}$  corresponding to the contribution of the  $m^{\text{th}}$   $q$ -channel bound state vanishes for  $m > 0$ :

$$\mathcal{F}_{m,00} = 2 \int_0^\infty dz z^3 e^{-z^2} L_m^1(z^2) = \delta_{m0}. \quad (49)$$

In the case of  $F_{00}(Q^2)$  form factor, we have

$$\begin{aligned} F_{00}(Q^2) &= \frac{1}{(1+a)(1+a/2)} \\ &= \frac{2}{1+Q^2/M_0^2} - \frac{1}{1+Q^2/M_1^2}. \end{aligned} \quad (50)$$

Thus, the  $F_{00}(Q^2)$  form factor is given by contributions from the lowest two  $q$ -channel bound states. Since  $F_{00}(Q^2) \sim 1/Q^4$  for large  $Q^2$ , exact VMD is impossible for this form factor: other resonances are needed to ‘‘conspire’’ to cancel their leading  $1/Q^2$  terms at large  $Q^2$ . In the soft-wall model, this cancellation is provided by just the first excited state.

For small  $Q^2$ , the form factor  $F_{00}^S(Q^2)$  has the following expansion:

$$F_{00}(Q^2) = \left[ 1 - \frac{3}{2} \frac{Q^2}{M_0^2} + \frac{7}{4} \frac{Q^4}{M_0^4} + \mathcal{O}(Q^6) \right]. \quad (51)$$

The Lorentz structure of the 3-point function in the soft-wall model is the same as in the hard-wall model considered in Ref. [18], where it was shown that electric  $G_C$ , magnetic  $G_M$  and quadrupole  $G_Q$  form factors (for definitions, see, e.g., [18, 21]) of the  $n^{\text{th}}$  bound state are all expressed through the  $F_{nn}(Q^2)$  form factor:

$$G_Q^{(n)}(Q^2) = -F_{nn}(Q^2), \quad G_M^{(n)}(Q^2) = 2F_{nn}(Q^2), \quad (52)$$

$$G_C^{(n)}(Q^2) = \left( 1 - \frac{Q^2}{6M^2} \right) F_{nn}(Q^2).$$

The same relations hold for the soft-wall model. As a result, small- $Q^2$  expansion of the electric form factor of the lowest bound state in the soft-wall model is given by

$$\begin{aligned} G_{00}(Q^2) &= \left[ 1 - \frac{Q^2}{6M_0^2} \right] F_{00}(Q^2) \\ &= \left[ 1 - \frac{5}{3} \frac{Q^2}{M_0^2} + 2 \frac{Q^4}{M_0^4} + \mathcal{O}(Q^6) \right], \end{aligned} \quad (53)$$

and the electric radius for the  $\rho$ -meson in the soft-wall model is

$$\langle r_\rho^2 \rangle^S = 0.655 \text{ fm}^2. \quad (54)$$

This radius is larger than the value  $\langle r_\rho^2 \rangle^H = 0.53 \text{ fm}^2$  that we obtained in Ref. [18] in the case of the hard-wall cutoff.

The radius of the  $n^{\text{th}}$  excited state can be found from the slope of  $F_{nn}(Q^2)$ . The latter can be calculated using Eqs. (7), (34). Defining the slope coefficient  $S_n$  by

$$\left. \frac{d}{dQ^2} F_{nn}(Q^2) \right|_{Q^2=0} \equiv -\frac{S_n}{M_0^2} \quad (55)$$

and using explicit form of Laguerre polynomials, we find

$$S_n = \sum_{m,l=0}^n C_{n+1}^{m+1} C_{n+1}^{l+1} (-1)^{l+m} \frac{(m+l+1)!}{(n+1)m!l!} \sum_{p=1}^{m+l+2} \frac{1}{p} \quad (56)$$

( $C_\alpha^\beta$  are binomial coefficients). A faster algorithm for numerical calculations is provided by the formula

$$S_n = \sum_{m=0}^n C_n^m C_{m+n+1}^n \sum_{k=0}^{n-m} C_{n-m}^k (-2)^k \sum_{p=1}^{2m+k+2} \frac{1}{p}. \quad (57)$$

For  $n = 0$ , these expressions give the result  $S_0 = 3/2$  corresponding to Eq. (51). For higher states, we have  $S_1 = 23/12$ ,  $S_2 = 11/5$ ,  $S_3 \approx 2.415$ ,  $S_{10} \approx 3.245$ ,  $S_{20} \approx 3.816$ ,  $S_{50} \approx 4.633$ ,  $S_{100} \approx 5.281$ ,  $S_{150} \approx 5.667$ ,  $S_{200} \approx 5.943$ . For  $n \geq 2$ , these values are well approximated by a simple empirical formula

$$S_n \approx \ln(n+1) + \frac{2}{3} + \frac{5}{4(n+1)}. \quad (58)$$

Thus, the squared sizes of excited states increase with the excitation number  $n$ . However, contrary to expectations of Ref. [12], the raise is only logarithmic,  $\langle r_n^2 \rangle^S \sim \ln n$  rather than linear. Such an outcome is not unnatural since Eq. (56) differs from the identity

$$\sum_{m,l=0}^n C_{n+1}^{m+1} C_{n+1}^{l+1} (-1)^{l+m} \frac{(m+l+1)!}{(n+1)m!l!} = 1 \quad (59)$$

(that follows from the normalization condition (9)) by the sum

$$\sum_{p=1}^{m+l+2} \frac{1}{p} \Big|_{m+l \rightarrow \infty} \sim \ln(m+l+2) \quad (60)$$

which has a logarithmic behavior for large  $m+l$ , and for large  $n$  it may be approximated by  $\ln n$  for the bulk of  $m, l$  values. However, it would be interesting to derive a formal proof.

It should be noted, that in the hard-wall model, the slope of  $F_{nn}(Q^2)$  at  $Q^2 = 0$  decreases with  $n$ . For the lowest state, the value  $S_1^H = 1.192$  was found in Ref. [18]. For higher radial excitations, we have  $S_2^H = 0.877$ ,  $S_3^H = 0.833$ ,  $S_{10}^H = 0.806$ ,  $S_{20}^H = 0.804$ ,  $S_{100}^H = 0.803$ , i.e.,  $\langle r_n^2 \rangle^H$  tends to a constant value as  $n \rightarrow \infty$ .

## VI. COMPARISON WITH HARD-WALL MODEL

Note that in the hard-wall model considered in Ref. [18], all the  $q$ -channel states give nonzero contributions to  $\mathcal{F}_{00}(Q^2)$ . In fact, it is strongly dominated by *two* lowest  $q$ -channel states. The role of the first excitation in the hard-wall model is especially important for large  $Q^2$ : it gives asymptotically  $2.061 M_\rho^2/Q^2$  while the lowest state contributes only  $0.619 M_\rho^2/Q^2$ .

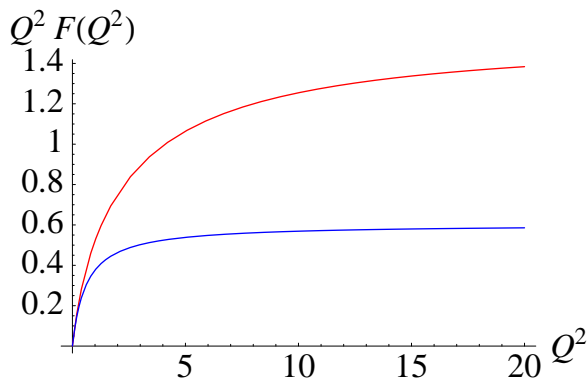


FIG. 1:  $Q^2$ -multiplied  $\rho$ -meson form factor  $\mathcal{F}_{00}(Q^2)$  (displayed in  $\text{GeV}^2$ ) as a function of  $Q^2$  (given in  $\text{GeV}^2$ ) in hard-wall (upper line, red online) and soft-wall (lower line, blue online) models.

It should also be mentioned that in both models  $\mathcal{F}_{00}(Q^2)$  has  $\sim 1/Q^2$  behavior for large  $Q^2$ . However, the normalization of the asymptotic behavior in hard-wall model is much larger than in soft-wall model:  $\mathcal{F}_{00}^H(Q^2) \rightarrow 2.566 M_\rho^2/Q^2$ , while  $\mathcal{F}_{00}^S(Q^2) \rightarrow M_\rho^2/Q^2$ .

As discussed in Refs. [15, 18], to calculate the large- $Q^2$  behavior of  $\mathcal{F}_{00}^H(Q^2)$ , one should take the large- $Q^2$  limit of  $\mathcal{J}^H(Q, z)$ , which is given by  $zQK_1(zQ) \equiv \mathcal{K}(Qz)$ , the free-field version of the nonnormalizable mode. Asymptotically, it behaves like  $e^{-Qz}$ , so only small values of  $z$  are important in the relevant integral. As a result,

$$\mathcal{F}_{00}^H(Q^2) \rightarrow \frac{|\Phi_0^H(0)|^2}{Q^2} \int_0^\infty d\chi \chi^2 K_1(\chi) = \frac{2|\Phi_0^H(0)|^2}{Q^2}, \quad (61)$$

i.e., the large- $Q^2$  behavior of  $\mathcal{F}_{00}^H(Q^2)$  is determined by the value of the  $\Phi$  wave function at the origin, which is

given by

$$\Phi_0^H(0) = \frac{\sqrt{2}M_\rho}{\gamma_{0,1}J_1(\gamma_{0,1})} \approx 1.133 M_\rho. \quad (62)$$

The nonnormalizable mode  $\mathcal{J}^S(Q, z)$  of the soft-wall model should also convert into  $\mathcal{K}(Qz)$  when  $Q^2$  is large. To see this directly, we compare the integral representation

$$\mathcal{K}(Qz) = z^2 \int_0^1 \frac{dx}{(1-x)^2} \exp\left[-\frac{(1-x)Q^2}{4x} - \frac{xz^2}{1-x}\right] \quad (63)$$

for  $\mathcal{K}(Qz)$  and the representation

$$\mathcal{J}^S(Q, z) = z^2 \int_0^1 \frac{dx}{(1-x)^2} \exp\left[-\frac{Q^2}{4} \ln\left(\frac{1}{x}\right) - \frac{xz^2}{1-x}\right] \quad (64)$$

for  $\mathcal{J}^S(Q, z)$  following from Eq. (14). For large  $Q^2$ , both integrals are dominated by the region where  $1-x \sim 2z\kappa^2/Q$ . Then both  $(1-x)/x$  and  $\ln(1/x)$  may be approximated by  $(1-x)$ . Thus, large- $Q^2$  behavior of  $\mathcal{J}^S(Q, z)$  coincides with that of  $\mathcal{K}(Qz)$ , and Eq. (61) is applicable in soft-wall model as well, with the normalization of the asymptotically leading term determined by the value of  $\Phi_0^S(z)$  at the origin, which is

$$\Phi_0^S(0) = M_\rho/\sqrt{2} \approx 0.707 M_\rho. \quad (65)$$

Hence, it is the difference in the values of  $\Phi$  wave functions at the origin that explains the difference in the asymptotic normalization of  $\mathcal{F}_{00}(Q^2)$  in these two models.

The difference in the values of  $\Phi(0)$  leads also to difference in the values of coupling constants  $f_n$  related to  $\Phi_n(0)$  by

$$f_n = \Phi_n(0)M_n/g_5. \quad (66)$$

The constant  $g_5$  is determined by matching the asymptotic behavior

$$\Sigma^{\text{AdS}}(p^2) \rightarrow -\frac{p^2}{2g_5^2} \ln(p^2) \quad (67)$$

of the two-point function  $\Sigma^{\text{AdS}}(p^2)$  given by Eq. (20) with the QCD result for the correlator of the vector currents  $J_\mu = \bar{d}\gamma_\mu u$  having quantum numbers of the  $\rho^+$  meson. Since

$$\Sigma^{\text{QCD}}(p^2) \rightarrow -\frac{N_c}{12\pi^2} p^2 \ln(p^2), \quad (68)$$

we have

$$g_5 = \sqrt{2}\pi \quad (69)$$

for  $N_c = 3$ . This gives

$$f_\rho^S = \frac{M_\rho^2}{2\pi} \approx (309 \text{ MeV})^2 \quad (70)$$

for the  $\rho$  coupling constant in the soft-wall model, and

$$f_\rho^H = \frac{M_\rho^2}{\pi\gamma_{0,1}J_1(\gamma_{0,1})} \approx (392 \text{ MeV})^2 \quad (71)$$

in the hard-wall model [28]. The experimental value [22]

$$f_\rho^{\text{exp}} = (401 \pm 4 \text{ MeV})^2 \quad (72)$$

is very close to the hard-wall model result, and in this respect the hard-wall model is more successful. It may be also noted that, unlike the value  $\langle r_\rho^2 \rangle^S = 0.655 \text{ fm}^2$  in Eq. (54), the hard-wall model result  $\langle r_\rho^2 \rangle^H = 0.53 \text{ fm}^2$  for the  $\rho$ -meson charge radius obtained in our paper [18] practically coincides both with the Dyson-Schwinger model result of Ref. [23] and lattice gauge calculation reported in Ref. [24].

It is also instructive to consider the modified coupling  $g_\rho \equiv f_\rho/M_\rho$  that has the dimension of mass, and determines the asymptotical behavior of the form factor. Its value in the soft-wall model

$$g_\rho^S = \frac{M_\rho}{2\pi} \approx 123 \text{ MeV} \quad (73)$$

is close to the experimental value of the pion decay constant  $f_\pi \approx 131 \text{ MeV}$ . Moreover, the pure  $\rho$ -pole result (48) is close to the experimental data on the pion form factor. So, it is tempting to take for the pion the same wave functions that were obtained in the  $\rho$ -meson case and use Eq. (48) as a model for the pion form factor. This was done in the paper [25] (that appeared after we submitted the original version [26] of the present paper to the archive). Taking  $\kappa = 375 \text{ MeV}$  (which is slightly smaller than  $m_\rho/2$ ), the authors obtained good agreement of the  $1/(1 + Q^2/4\kappa^2)$  curve with the pion form factor data (though the value of  $f_\pi^2$  is then about 30% below the experimental one). However, within the model of Refs. [6, 8, 12], which we follow here, the analysis of the axial-vector current channel requires the inclusion of chiral symmetry breaking effects absent in the vector current channel. As a result, wave function equations for the pion are completely different from those for the  $\rho$ -meson. We discuss the pion form factor in a separate publication [27].

## VII. SUMMARY

In the present paper, we studied wave functions and form factors of vector mesons within the framework of the soft-wall model [12] which produces a more realistic spectrum for higher excited mesons [19] than the hard-wall model of Refs. [6, 7, 8]. Our analysis uses the approach similar to that we developed in Ref. [18] in application to the hard-wall model.

An essential element of our study of the soft-wall model is the integral representation, which we found for the bulk-to-boundary propagator  $\mathcal{V}(p, z)$ . It allows to write

$\mathcal{V}(p, z)$  as an explicit expansion over bound state poles. In this sense, it plays the same role as the Kneser-Sommerfeld expansion that we used in our study [18] of the hard-wall model.

The pole expansion of  $\mathcal{V}(p, z)$  involves “ $\psi$  wave functions” that describe  $z$ -dependence of a particular pole contribution and are eigenfunctions of the 5D equation of motion. However, since  $\psi_n(z)$  wave functions are not direct analogues of the usual quantum-mechanical wave functions, we introduced “ $\Phi$  wave functions” resembling wave functions of oscillator states in quantum mechanics. In particular, the values of these functions at the origin give the couplings  $g_5 f_n/M_n$  of the bound states, and these functions exponentially decrease with  $z^2$ .

Analyzing the three-point function, we obtained expressions for transition form factors both in terms of the  $\psi$  wave functions and the “more physical”  $\Phi$  wave functions. We demonstrated that, just like in the hard-wall model, the form factors can be written in the form of generalized vector meson dominance representation, i.e., as a sum over all bound states in the channel of electromagnetic current (this result confirms the claim [16] that generalized VMD is a common feature of AdS/QCD models).

We derived an explicit expression for  $\rho$ -meson form factors, and analyzed their behavior in the regions of small and large  $Q^2$ . In particular, we calculated the  $\rho$ -meson electric radius in the soft-wall model, and found that it is larger than in the hard-wall model (the latter agrees with calculations in Dyson-Schwinger model [23] and lattice QCD [24]). Our calculation also demonstrated that the squared radii of higher excited states increase with  $n$ , the number of the radially excited level. However, contrary to expectations of Ref. [12], the increase is only logarithmic rather than linear. Another result is that, in the soft-wall model, the  $\rho$ -meson form factor  $\mathcal{F}_\rho(Q^2)$  (corresponding to the overlap of the  $\Phi$  wave functions) exhibits an exact VMD pattern, i.e., it is given by a single monopole term due to the lowest bound state in the  $Q^2$ -channel. In the case of the  $\rho$ -meson form factor  $F_\rho(Q^2)$  (that is given by the overlap of the  $\psi$ -wave functions), we found a two-resonance dominance pattern, when just two lowest bound states in the  $Q^2$ -channel contribute.

Analyzing the large- $Q^2$  behavior of the  $\mathcal{F}_\rho(Q^2)$  form factor (given by exact  $\rho$ -pole VMD), we established that its asymptotic normalization in the soft-wall model is much lower (by factor 2.566) than that of the hard-wall model. This difference is explained by essentially lower value of the soft-wall model  $\Phi$  wave function at the origin.

Finally, we calculated the  $\rho$ -meson coupling constant  $f_\rho$  both in the soft-wall and hard-wall models, and found that the experimental value is closer to the hard-wall model result.

## Acknowledgments

H.G. would like to thank J. Erlich for discussions, A. W. Thomas for support at Jefferson Laboratory and J. P. Draayer for support at Louisiana State University.

A.R. thanks S. J. Brodsky and J. P. Vary for useful discussions.

Notice: Authored by Jefferson Science Associates, LLC under U.S. DOE Contract No. DE-AC05-06OR23177.

The U.S. Government retains a non-exclusive, paid-up, irrevocable, world-wide license to publish or reproduce this manuscript for U.S. Government purposes.

- 
- [1] J. M. Maldacena, *Adv. Theor. Math. Phys.* **2**, 231 (1998) [*Int. J. Theor. Phys.* **38**, 1113 (1999)]; S. S. Gubser, I. R. Klebanov and A. M. Polyakov, *Phys. Lett. B* **428**, 105 (1998); E. Witten, *Adv. Theor. Math. Phys.* **2**, 253 (1998)
- [2] J. Polchinski and M. J. Strassler, *Phys. Rev. Lett.* **88**, 031601 (2002); *JHEP* **0305**, 012 (2003)
- [3] H. Boschi-Filho and N. R. F. Braga, *JHEP* **0305**, 009 (2003); *Eur. Phys. J. C* **32**, 529 (2004).
- [4] S. J. Brodsky and G. F. de Téramond, *Phys. Lett. B* **582**, 211 (2004); G. F. de Téramond and S. J. Brodsky, *Phys. Rev. Lett.* **94**, 201601 (2005)
- [5] T. Sakai and S. Sugimoto, *Prog. Theor. Phys.* **113**, 843 (2005); **114**, 1083 (2006)
- [6] J. Erlich, E. Katz, D. T. Son and M. A. Stephanov, *Phys. Rev. Lett.* **95**, 261602 (2005)
- [7] J. Erlich, G. D. Kribs and I. Low, *Phys. Rev. D* **73**, 096001 (2006)
- [8] L. Da Rold and A. Pomarol, *Nucl. Phys. B* **721**, 79 (2005); *JHEP* **0601**, 157 (2006)
- [9] K. Ghoroku, N. Maru, M. Tachibana and M. Yahiro, *Phys. Lett. B* **633**, 602 (2006)
- [10] J. Hirn and V. Sanz, *JHEP* **0512**, 030 (2005); J. Hirn, N. Rius and V. Sanz, *Phys. Rev. D* **73**, 085005 (2006)
- [11] S. J. Brodsky and G. F. de Téramond, *Phys. Rev. Lett.* **96**, 201601 (2006)
- [12] A. Karch, E. Katz, D. T. Son and M. A. Stephanov, *Phys. Rev. D* **74**, 015005 (2006)
- [13] C. Csaki and M. Reece, arXiv:hep-ph/0608266.
- [14] T. Hambye, B. Hassanain, J. March-Russell and M. Schwelling, *Phys. Rev. D* **74**, 026003 (2006); arXiv:hep-ph/0612010.
- [15] A. V. Radyushkin, *Phys. Lett. B* **642**, 459 (2006)
- [16] S. Hong, S. Yoon and M. J. Strassler, *JHEP* **0604**, 003 (2006);
- [17] S. Hong, S. Yoon and M. J. Strassler, arXiv:hep-ph/0501197.
- [18] H. R. Grigoryan and A. V. Radyushkin, *Phys. Lett. B* **650**, 421 (2007).
- [19] M. Shifman, arXiv:hep-ph/0507246.
- [20] E. Schreiber, arXiv:hep-th/0403226.
- [21] R. G. Arnold, C. E. Carlson and F. Gross, *Phys. Rev. C* **21**, 1426 (1980).
- [22] S. Eidelman *et al.* [Particle Data Group], *Phys. Lett. B* **592**, 1 (2004); H. M. Choi and C. R. Ji, *Phys. Rev. D* **75**, 034019 (2007).
- [23] M. S. Bhagwat and P. Maris, arXiv:nucl-th/0612069.
- [24] B. G. Lasscock, J. Hedditch, D. B. Leinweber and A. G. Williams, *PoS LAT2006*, 114 (2006) [arXiv:hep-lat/0611029].
- [25] S. J. Brodsky and G. F. de Téramond, arXiv:0707.3859 [hep-ph].
- [26] H. R. Grigoryan and A. V. Radyushkin, arXiv:0706.1543 [hep-ph].
- [27] H. R. Grigoryan and A. V. Radyushkin, arXiv:0709.0500 [hep-ph].
- [28] The hard-wall model result  $F_\rho^{1/2} \approx 329 \text{ MeV}$  presented in Ref. [6] corresponds to the  $(\bar{u}\gamma_\mu u - \bar{d}\gamma_\mu d)/2$  current which differs by  $\sqrt{2}$  from the current  $(\bar{u}\gamma_\mu u - \bar{d}\gamma_\mu d)/\sqrt{2}$  that has the same normalization as  $\bar{d}\gamma_\mu u$ .